

# Relationship between X-ray spectral index and X-ray Eddington ratio for Mrk 335 and Ark 564

R. Sarma<sup>1\*</sup>, S. Tripathi<sup>2</sup>, R. Misra<sup>2</sup>, G. Dewangan<sup>2</sup>, A. Pathak<sup>3</sup> and J. K. Sarma<sup>3</sup>

<sup>1</sup>*Department of Physics, Hojai College, Hojai, 782435, India*

<sup>2</sup>*Inter-University Centre For Astronomy and Astrophysics, Post Bag 4, Ganeshkind, Pune-411007, India*

<sup>3</sup>*Department of Physics, Tezpur University, 784028, India*

## ABSTRACT

We present a comprehensive flux resolved spectral analysis of the bright Narrow line Seyfert I AGNs, Mrk 335 and Ark 564 using observations by XMM-Newton satellite. The mean and the flux resolved spectra are fitted by an empirical model consisting of two Comptonization components, one for the low energy soft excess and the other for the high energy power-law. A broad Iron line and a couple of low energies edges are required to explain the spectra. For Mrk 335, the 0.3 - 10 keV luminosity relative to the Eddington value,  $L_X/L_{Edd}$ , varied from 0.002 to 0.06. The index variation can be empirically described as  $\Gamma = 0.6 \log_{10} L_X/L_{Edd} + 3.0$  for  $0.005 < L_X/L_{Edd} < 0.04$ . At  $L_X/L_{Edd} \sim 0.04$  the spectral index changes and then continues to follow  $\Gamma = 0.6 \log_{10} L_X/L_{Edd} + 2.7$ , i.e. on a parallel track. We confirm that the result is independent of the specific spectral model used by fitting the data in the 3 - 10 keV band by only a power-law and an Iron line. For Ark 564, the index variation can be empirically described as  $\Gamma = 0.2 \log_{10} L_X/L_{Edd} + 2.7$  with a significantly large scatter as compared to Mrk 335. Our results indicate that for Mrk 335, there may be accretion disk geometry changes which lead to different parallel tracks. These changes could be related to structural changes in the corona or enhanced reflection at high flux levels. There does not seem to be any homogeneous or universal relationship for the X-ray index and luminosity for different AGNs or even for the same AGN.

**Key words:** Key Words: galaxies: Seyfert, X-rays: galaxies

## 1 INTRODUCTION

Active Galactic Nuclei (AGN) are known to emit X-rays as a result of physical processes active in the innermost regions near the central super-massive black hole. X-ray spectra of a typical AGN in the 2-10 keV range show primarily the signature of a power-law continuum and an iron line. At energies  $< 2$  keV there is often a soft excess over the power-law emission. The power-law emission is widely considered as the outcome of inverse Compton scattering of thermally produced accretion disk seed optical/UV photons by a corona of hot electrons close to the disc (Haardt & Maraschi 1991, 1993; Zdziarski, Poutanen, & Johnson 2000). However, the geometry and size of the corona as well as the physical mechanism governing the energy transfer between the two phases are not well understood.

While, the average value of photon index of the primary power-law for AGN has been found to be  $\Gamma \sim 1.9$ , there is a large variation with  $\Gamma$  ranging from 1.5-2.5 (Nandra & Pounds 1994; Page et al. 2005). For a given

AGN,  $\Gamma$  varies as a function of time. Understanding the behaviour of  $\Gamma$  with other source properties is expected to give important insight into the nature of the radiative mechanism and the geometry of the inner regions.

Previous studies have shown the existence of a correlation between the X-ray photon index  $\Gamma$  and the source flux e.g., (Perola et al. 1986; Singh, Rao & Vahia 1991; Mushotzky et al. 1993; Done, Madejski, & Życki 2000; Nandra & Papadakis 2001). For many Seyfert 1 AGNs, the power-law index shows significant variation and generally follows the trend of steeper  $\Gamma$  with increasing source intensity. During 1997, MCG 6-30-15 was observed with *RXTE* for a duration of 8 days  $\sim 910$  ks. The range of  $\Gamma$  observed was 1.8-2.2 with flux variation of  $\sim 3.3$  in the energy band 2-10 keV. This observation showed a tight correlation between the photon index  $\Gamma$  and the source flux in the sense that the power-law steepens as the source gets brighter (Vaughan & Edelson 2001). The steepening of  $\Gamma$  (range 1.89-2.34) with flux has also been observed in IRAS 13224-3809, where a 10 day long *ASCA* observation revealed a change in the power-law flux by a factor of  $\sim 3.2$  in the 2-10 keV range (Dewangan et al. 2002). *RXTE* observed NGC 5548 on five

\* e-mail: sharma.rathin@gmail.com

occasions in 1998 during which a clear positive correlation between the photon index (range 1.75-1.93) and the 2-10 keV flux was seen with flux variation of  $\sim 1.84$ . (Chiang et al. 2000). For the soft energy band (0.3-2.0 keV), similar trend between photon index (range 1.7-2.0) and flux was observed for a 2 day long *BEPOSAX* observation of 3C 120 with flux variation of  $\sim 1.5$  (Zdziarski & Grandi 2001). The Seyfert galaxy NGC 4151 was observed on seven occasions by *Ginga* during May 1987-January 1989 ( $\sim 21$  months). In this observation significant flux variation ( $\sim 3$ ) has been seen along with the correlation between the photon index and flux (Yaqoob & Warwick 1991). The 2009 *XMM-Newton* observation of Mrk 335 has also shown ‘softer when brighter’ property (Grupe et al. 2012). In all the above examples of AGNs, the flux variation during the observations does not exceed a factor of  $\sim 4$ .

Studies of a sample of AGNs have also provided evidence that there is significant positive correlation between the X-ray photon index and the bolometric Eddington ratio,  $\lambda = L_{Bol}/L_{Edd}$ , where  $L_{Edd}$  is the Eddington luminosity (Laor et al. 1997; Lu & Yu 1999; Wang, Watarai, & Mineshige 2004; Shemmer et al. 2006). With larger samples involving sources with higher redshifts and greater luminosities, it was observed that the hard X-ray photon index correlates with the bolometric Eddington ratio when  $\lambda \gtrsim 0.01$  (Porquet et al. 2004; Shemmer et al. 2006; Saez et al. 2008; Sobolewska & Papadakis 2009; Cao 2009; Zhou, Xin, & Zhao 2010; Liu et al. 2012; Brightman et al. 2013) but when  $\lambda < 0.01$ , especially for low-luminosity AGNs, anti-correlation is seen between  $\Gamma$  and  $\lambda$  (Gu & Cao 2009; Constantin et al. 2009; Younes et al. 2011; Xu 2011). In general, there have been several studies to investigate the relation between the photon index and  $\lambda$  for different samples of AGN (e.g. Risaliti, Young, & Elvis 2009; Jin, Ward, & Done 2012). Studies incorporating *ROSAT* and *ASCA* observations showed the correlation between  $\Gamma$  and full width at half maximum (FWHM) of the  $H\beta$  emission line (Boller, Brandt, & Fink 1996; Brandt, Mathur, & Elvis 1997; Dewangan et al. 2002).

There is a need to study the relation between spectral index and Eddington ratio spanning a larger range in  $L/L_{Edd}$ . This is provided by *XMM-Newton* data for the bright and highly variable Narrow Line Seyfert 1 (NLS1) galaxy Mrk 335. For comparison we also analyse the extensive data available for another NLS1, Ark 564.

Narrow line Seyfert 1 galaxies (NLS1) form a subset of AGN which exhibit exceptional features in terms of emission-line and continuum properties. Unlike Seyfert 2 galaxies which show narrow optical emission lines, NLS1 show the broad emission-line optical spectra of Seyfert 1 galaxies, but with the narrowest Balmer lines from the broad line region (full width at half maximum (FWHM)  $\lesssim 2000 \text{ km s}^{-1}$  with relatively weak [OIII] $\lambda 5007$  emission) and prominent optical Fe II emission (Osterbrock & Pogge 1985; Véron-Cetty, Véron, & Gonçalves 2001). NLS1 also show a number of other extreme properties in X-rays e.g., strong soft excess emission below 1 keV, steep 2-10 keV power-law continuum and very rapid and large X-ray variability (Leighly 1999; Gallo et al. 2004). Their X-ray spectra often present complex behaviour with the presence of cold and ionised absorption, partial covering and reflection components ((Komossa 2008) and references therein). Also NLS1

galaxies as a class follow the  $M_{BH} - \sigma_*$  relation if the widths of emission lines not strongly affected by outflow components are used as a surrogate for  $\sigma_*$  (Komossa & Xu 2007). Due to all these extreme and ambiguous properties, NLS1 as a special class of AGN seem to challenge the Unified model and need a more careful investigation. Recent observations and surveys have pointed towards the presence of smaller black hole masses in NLS1 galaxies (Barth, Greene, & Ho 2005; Botte et al. 2004) and which could possibly represent an important connection with the less explored intermediate mass black holes. It is believed that the extreme X-ray and other observed properties of NLS1 galaxies may be due to an extreme value of a fundamental physical parameter related to the accretion process. This fundamental parameter is most likely to be the accretion rate relative to the Eddington rate. This is well supported by more recent studies, theoretical considerations and by black hole mass estimates from optical emission-line and continuum measurements that NLS1 are accreting close to their Eddington rates (Boller, Brandt, & Fink 1996; Boroson 2002; Xu et al. 2003; Grupe 2004; Warner, Hamann, & Dietrich 2004; Collin et al. 2006) and hence should be considered important testbeds of accretion models. Recent X-ray study of NLS1 using an optically selected SDSS sample have shown that some NLS1 show steep X-ray spectra and strong Fe II emission while some do not. In this study, a strong correlation was also found between  $\Gamma$  and the luminosity at 1 keV,  $L_{1keV}$  suggesting differences in  $L_{bol}/L_{Edd}$  among the NLS1s in the sample (Williams, Pogge, & Mathur 2002; Williams, Mathur, & Pogge 2004).

Mrk 335, also known as PG003+199 is a nearby NLS1 galaxy at a redshift  $z=0.026$  (Longinotti et al. 2007a) and has a well measured black hole mass of  $1.4 \times 10^7 M_{\odot}$  from reverberation mapping (Peterson et al. 2004; Grier et al. 2012). It has been the target of most X-ray observatories. *XMM-Newton* observed Mrk 335 for the first time in 2000. Analysing the RGS data, an absorption edge at 0.54 keV due to Galactic oxygen was reported and the soft excess was described as a combination of bremsstrahlung emission and ionised reflection from the accretion disk (Gondoin et al. 2002). The *XMM-Newton* observation was later reanalysed and a narrow absorption feature at 5.9 keV was found (Longinotti et al. 2007a). In 2006 January, *XMM-Newton* re-observed Mrk 335 for 133 ks which revealed a double-peaked Fe emission feature with peaks at 6.4 and 7.0 keV (O’Neill et al. 2007). (Larsson et al. 2008) studied Mrk 335 using a 151 ks *Suzaku* observation performed in 2006. They modelled the data using a power law and two reflectors in which an ionised, heavily blurred, inner reflector produces most of the soft excess, while an almost neutral outer reflector (outside  $\sim 40r_g$ ) produces most of the Fe line emission. They also verified their model using the 2006 *XMM-Newton* data and did not see any correlation between photon index and power law flux. But subsequently a marginal trend, i.e., the source becomes softer with increasing count rate has been reported for the same data (Grupe et al. 2012). When observed by *XMM-Newton* in July 2007 for 22 ks, Mrk 335 was found to be in extremely low X-ray flux state (Grupe et al. 2008). The spectrum of this low flux state of Mrk 335 was explained by partial covering and blurred reflection models. Mrk 335 was again observed by *XMM-Newton* in 2009 for 200 ks spread over two consecutive or-

bits. The X-ray continuum and timing properties have been described by using a blurred reflection model (Gallo et al. 2013). The 2009 *XMM-Newton* data have also been analysed by Grupe et al. (2012) along with the *Swift* data. Partial absorption and blurred reflection models gives equally good fit to the spectrum. The number of observations of Mrk 335 by *XMM-Newton* over time provides an opportunity to study the variation of the high energy photon index with luminosity in a systematic manner.

At a redshift  $z=0.02469$  (Huchra et al. 1999), Ark 564 is the brightest NLS1 galaxy in the 2.0-10.0 keV range,  $L_{(2-10)keV} = 2.4 \times 10^{43}$  erg s $^{-1}$  (Turner et al. 2001). Ark 564 has been studied across all wavebands (Shemmer et al. 2001; Romano et al. 2004). In the 2000 and 2001 *XMM-Newton* observations of Ark 564, Vignali et al. (2004) reported an edge-like feature in the EPIC data at  $\sim 0.73$  keV and interpreted it as the OVII K absorption edge. The  $\sim 100$  ks 2005 *XMM-Newton* observation of Ark 564 have been described as either a power law and two black-bodies or a relativistically blurred photo ionised disk reflection model (Papadakis et al. 2007). Dewangan et al. (2007) analysed the 2005 data and found two warm absorber phases. During 2011, Ark 564 has been observed by *XMM-Newton* for eight occasions. Legg et al. (2012) confirmed a significant soft lag in the 0.3-1.0 keV and 4.0-7.5 keV bands and suggested a distant reflection origin. Thus, Ark 564 has been also observed several times by *XMM-Newton* making it another good candidate.

Here we investigate the dependence of power-law index with the X-ray Eddington ratio for the combined EPIC spectra of Mrk 335 and Ark 564. Using flux resolved spectroscopy we study the power law index variation against X-ray Eddington ratio. The paper is organised as follows. Section 2 describes the observations and the data reduction procedure and Section 3 explains the spectral model used for the analysis. The details of the flux resolved spectroscopy are given in section 4. Finally, we conclude this work with a summary of the results and discussion in section 5.

## 2 OBSERVATIONS AND DATA REDUCTION

For the analysis, we use all the available archival data of Mrk 335 and Ark 564 from the *XMM-Newton* observatory (Jansen et al. 2001). The list of observations are shown in Table 1. The *XMM-Newton* data have been processed in the standard way using the SAS version 12.0. For all cases we have considered data from the EPIC-pn camera (Struder et al. 2001) only.

The data were cleaned for high background flares and were selected using the conditions  $PATTERN \leq 4$  and  $FLAG == 0$ . We have checked for pile-up in all cases using SAS task *epatplot* and found that for both the sources some observations are affected by pile-up (Table 1). We reduced the pile-up by excluding the innermost source emission using an annular region as considered by (Legg et al. 2012). Except for the pile-up affected observations, the source spectra have been extracted from circular regions of radius 35 arc s centred on the maximum source emission. The redistribution matrices and auxiliary response files were created by the SAS task *especget*. Spectra were grouped such that each bin contained at least 30 counts. Spectral fits to the data

**Table 1.** Observation log of Mrk 335 and Ark564 by *XMM-Newton*

Mrk 335			
OBS. ID	Duration(s)	Date	Pile-up
0101040101	36910	2000-12-25	yes
0306870101	133251	2006-01-03	no
0510010701	22580	2007-07-10	no
0600540601	132315	2009-06-11	no
0600540501	82615	2009-06-13	no
Ark 564			
0006810101	34466	2000-06-17	no
0006810301	16211	2001-06-09	no
0206400101	101774	2005-01-05	no
0670130201	59500	2011-05-24	yes
0670130301	55900	2011-05-30	no
0670130401	63620	2011-06-05	no
0670130501	67300	2011-06-11	yes
0670130601	60900	2011-06-17	no
0670130701	64420	2011-06-25	no
0670130801	58200	2011-06-29	yes
0670130901	55900	2011-07-0	yes

were performed with XSPEC version 12.8.0 (Arnaud 1996). The background subtracted light curves have been produced with the tool *EPICLCCORR* which are binned with 400 s bins.

## 3 PHENOMENOLOGICAL MODEL

We fit the EPIC-pn spectral data in the 0.3-10.0 keV range, by a simple phenomenological model consisting of two thermal Comptonization models. In particular, the soft excess is described by the XSPEC model “nthComp” and for the hard X-ray emission, we have used XSPEC convolution model “Simpl” (Steiner et al. 2008). Galactic absorption is taken to be  $N_H=3.99 \times 10^{20}$  cm $^{-2}$  for Mrk 335 and  $N_H=5.34 \times 10^{20}$  cm $^{-2}$  for Ark 564 (Kalberla et al. 2005). For Mrk 335 there are clear residuals at around  $\sim 6$  keV signifying the presence of a broad Iron line which we modelled using the “diskline” (Fabian et al. 1989). The inner radius of the line emitting region  $R_{in}$  is fixed at  $6r_g$  and the outer radius  $r_{out}$  is fixed at  $1000r_g$ . The inclination of the disk is fixed at  $40^\circ$ . For the “nthcomp” model we find that the results are not sensitive to the input seed photons which we fix to be a blackbody at 0.05 keV. For both the sources, addition of 2 or 3 low energy absorption edges improves the spectral fitting. For one of the Mrk 335 observations there is also a hint of a narrow emission line at 7 keV. Figure 1 presents the unfolded spectra for the observations 0101040101, 0306870101, 0600540501 and 0600540601 of Mrk 335. The best fit spectral parameters and the reduced  $\chi^2$  for all the observations are listed in Tables 2 and 3.

The reduced  $\chi^2$  of the fits to the observations range from 1 to 1.6, which suggests that the underlying spectra may be more complex than the phenomenological model used here, especially at low energies. However for the motivation of this work, the phenomenological model used here is adequate since even for a reduced  $\chi^2 \sim 1.6$ , the model

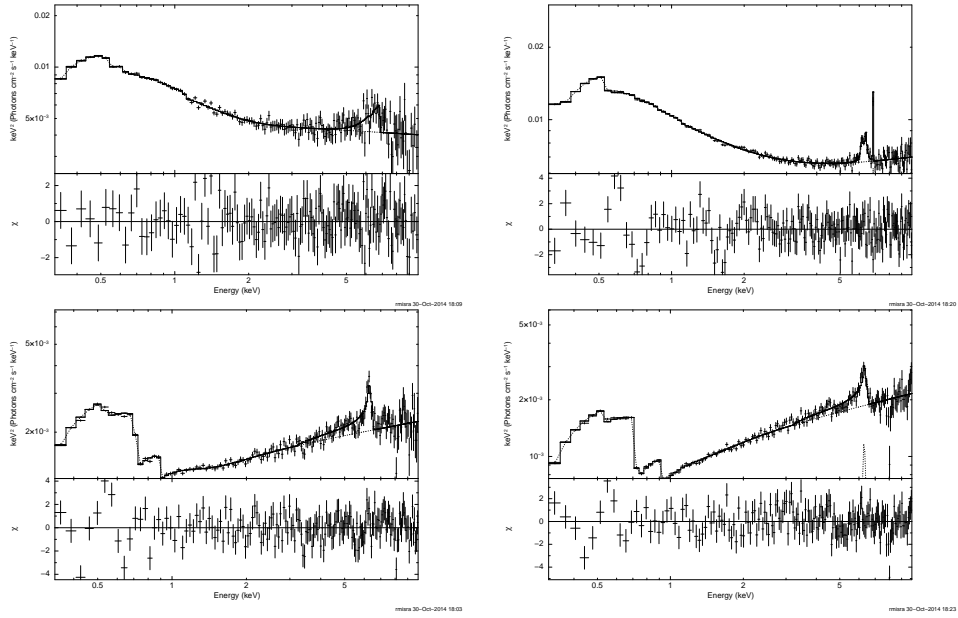


**Figure 1.** EPIC PN unfolded spectra and residuals ( $\Delta\chi$ ) of Mrk 335 observations i.e. 0101040101 (top right), 0306870101 (top left), 0600540501 (bottom right) and 0600540601 (bottom left) for the phenomenological model with best fit parameters listed in Table 2.

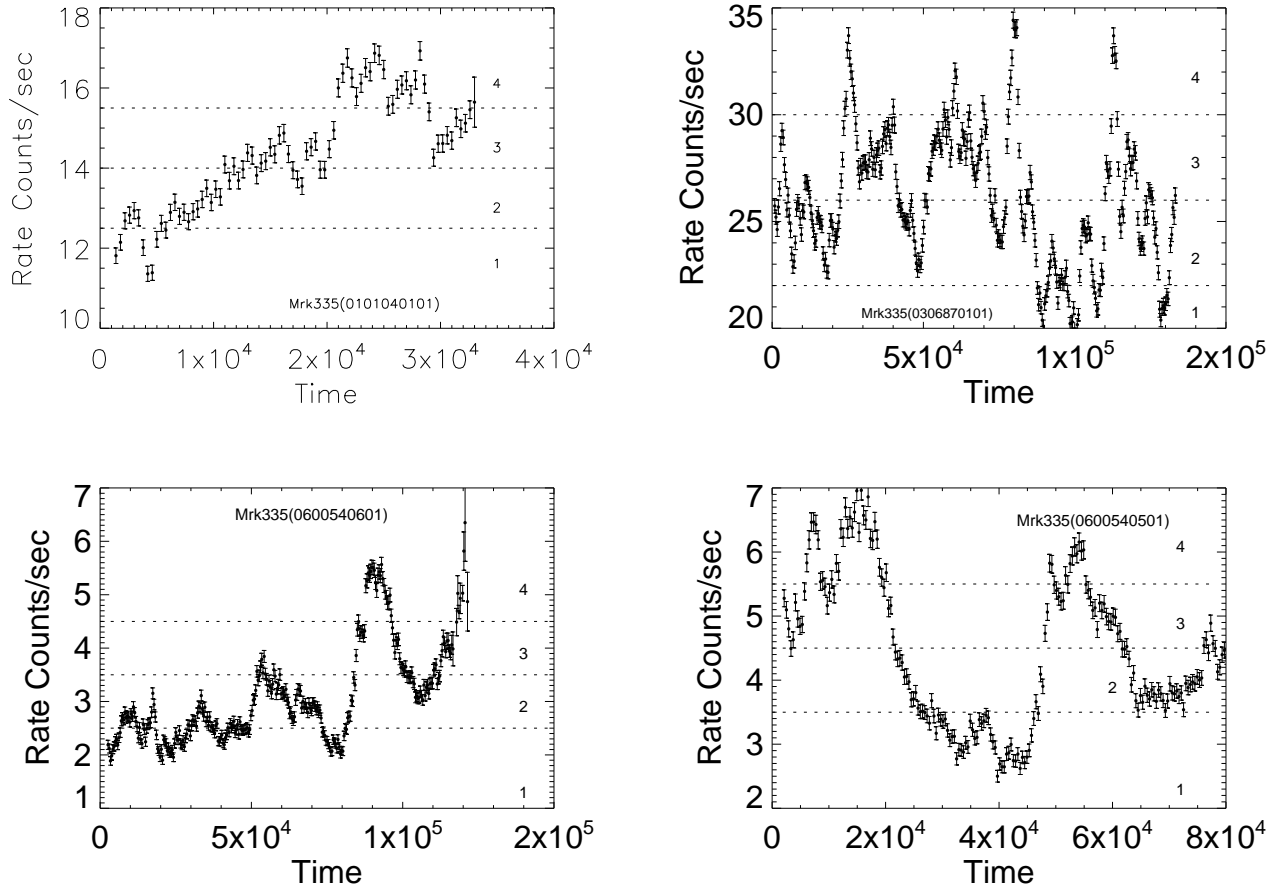


**Figure 2.** EPIC PN light curve (in 400 s bins) of Mrk 335. The light curves were extracted in the energy range of (0.3-10.0) keV. The time ranges for flux resolved spectroscopy have been selected corresponding to different counts  $s^{-1}$  as shown by the horizontal dotted lines.

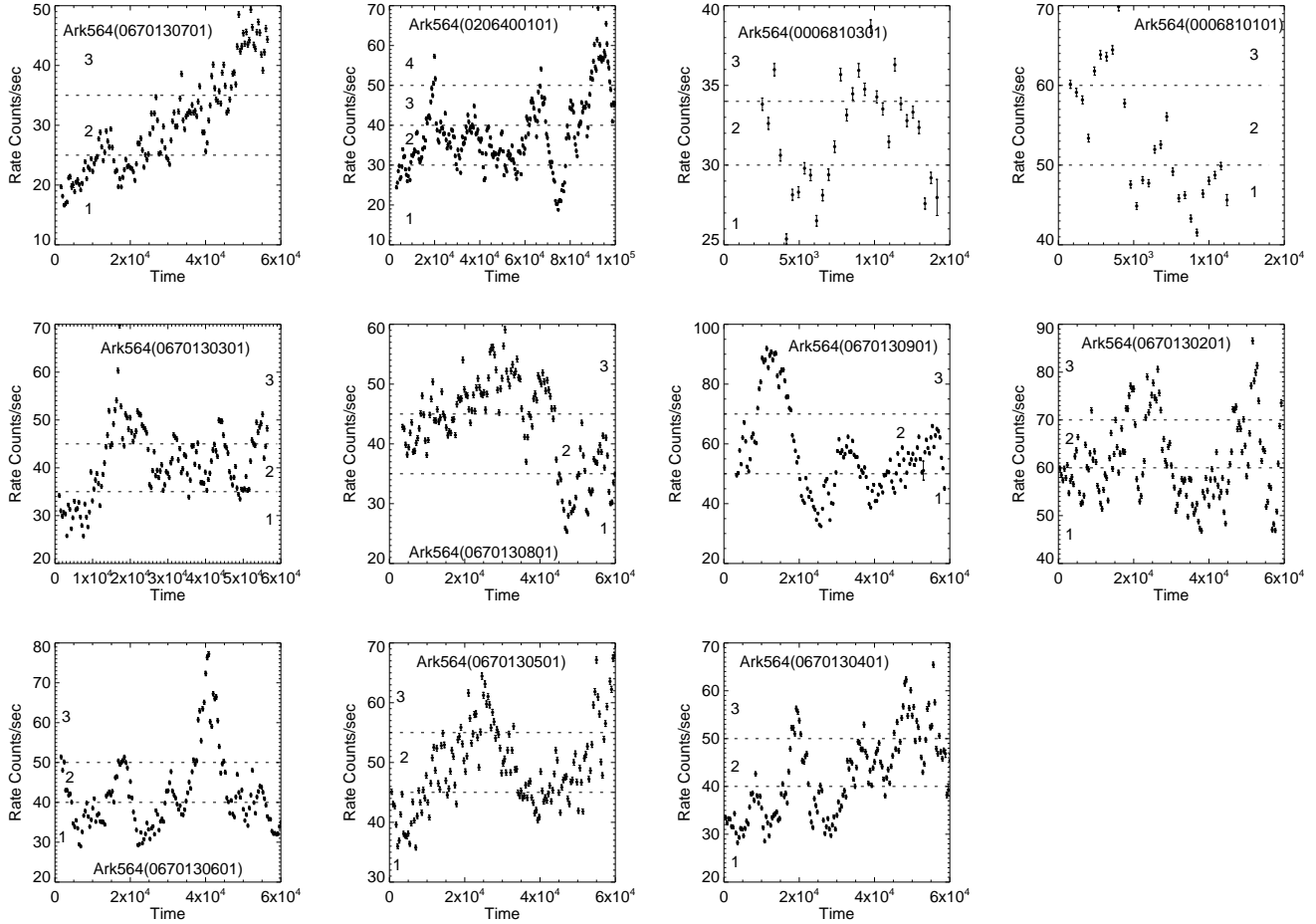


**Figure 3.** EPIC PN light curve (in 400 s bins) of Ark 564. The light curves were extracted in the energy range of (0.3-10.0) keV. The time ranges for flux resolved spectroscopy have been selected corresponding to different counts  $s^{-1}$  as shown by the horizontal dotted lines.

**Table 2.** Spectral parameters for Mrk 335 derived from different *XMM-Newton* observations in the (0.3-10.0)keV range.

Model	parameter	0101040101	0306870101	0510010701	0600540601	0600540501
zedge1	$E_c$ (keV)	0.63(froze)	$0.361^{+0.003}_{-0.004}$	$1.047^{+0.032}_{-0.035}$	$0.730^{+0.004}_{-0.003}$	$0.730^{+0.004}_{-0.004}$
	$\tau$	$0.097^{+0.028}_{-0.031}$	$0.228^{+0.027}_{-0.006}$	$0.369^{+0.091}_{-0.093}$	$0.776^{+0.027}_{-0.042}$	$0.553^{+0.029}_{-0.017}$
zedge2	$E_c$ (keV)	$1.127^{+0.042}_{-0.046}$	$1.120^{+0.034}_{-0.230}$	$1.509^{+0.060}_{-0.063}$	$0.943^{+0.011}_{-0.012}$	$0.922^{+0.014}_{-0.011}$
	$\tau$	$0.063^{+0.031}_{-0.031}$	$0.026^{+0.006}_{-0.006}$	$0.377^{+0.101}_{-0.095}$	$0.313^{+0.030}_{-0.041}$	$0.238^{+0.024}_{-0.040}$
zedge3	$E_c$ (keV)	-	-	0.686(Froze)	-	-
	$\tau$	-	-	$0.524^{+0.104}_{-0.100}$	-	-
Diskline <sup>†</sup>	$E_c$ (keV)	$6.313^{+0.362}_{-0.184}$	$6.275^{+0.032}_{-0.041}$	$6.009^{+0.056}_{-0.068}$	$6.022^{+0.050}_{-0.061}$	$5.952^{+0.070}_{-0.064}$
	$\beta$	$-2.609^{+0.749}_{-5.900}$	$-1.326^{+0.643}_{-0.414}$	$-9.668^{+3.607}_{-8.006}$	$-7.416^{+2.297}_{-4.753}$	$-5.061^{+1.497}_{-4.475}$
	Norm( $\times 10^{-4}$ )	$0.449^{+0.254}_{-0.168}$	$0.217^{+0.044}_{-0.038}$	$0.549^{+0.074}_{-0.076}$	$0.276^{+0.034}_{-0.033}$	$0.292^{+0.042}_{-0.022}$
zgaussian	$E_c$	-	$7.004^{+0.030}_{-0.031}$	-	-	-
	Norm( $\times 10^{-3}$ )	-	$0.007^{+0.002}_{-0.002}$	-	-	-
Simpl	$\Gamma$	$2.094^{+0.024}_{-0.049}$	$1.885^{+0.009}_{-0.005}$	$1.064^{+0.073}_{-0.046}$	$1.676^{+0.018}_{-0.007}$	$1.787^{+0.018}_{-0.008}$
	FracScat	$0.136^{+0.011}_{-0.009}$	$0.087^{+0.002}_{-0.001}$	$0.310^{+0.324}_{-0.104}$	$0.233^{+0.012}_{-0.007}$	$0.193^{+0.007}_{-0.005}$
nthComp	$\Gamma$	$2.862^{+0.052}_{-0.057}$	$3.277^{+0.008}_{-0.023}$	$1.980^{+0.094}_{-0.092}$	$1.922^{+0.087}_{-0.213}$	$2.043^{+0.069}_{-0.219}$
	kT(keV)	$0.266^{+0.051}_{-0.031}$	$0.823^{+0.019}_{-0.020}$	$0.210^{+0.019}_{-0.019}$	$0.153^{+0.008}_{-0.018}$	$0.159^{+0.008}_{-0.020}$
	Norm( $\times 10^{-2}$ )	$0.428^{+0.029}_{-0.032}$	$0.705^{+0.007}_{-0.037}$	$0.093^{+0.084}_{-0.039}$	$0.060^{+0.003}_{-0.008}$	$0.091^{+0.006}_{-0.009}$
reduced $\chi^2$ /d.o.f.		1.04/144	1.48/163	1.70/130	1.40/161	1.52/159

<sup>†</sup>The values of  $r_{in}$  and  $r_{out}$  have been fixed at  $6r_g$  and  $1000r_g$  respectively while the inclination has been fixed at  $40^\circ$ .



**Table 3.** Spectral parameters for Ark 564 derived from different *XMM-Newton* observations in the (0.3-10.0)keV range.

Model	Parameter	0006810101	0670130301	0670130801	0670130901	0670130201	0670130601
zedge1	$E_c$ (keV)	$0.508^{+0.013}_{-0.015}$	$0.708^{+0.008}_{-0.008}$	$0.345^{+0.013}_{-0.015}$	$0.723^{+0.010}_{-0.010}$	$0.330^{+0.011}_{-0.018}$	$0.347^{+0.005}_{-0.006}$
	$\tau$	$0.111^{+0.022}_{-0.022}$	$0.105^{+0.012}_{-0.010}$	$0.244^{+0.050}_{-0.051}$	$0.093^{+0.014}_{-0.013}$	$0.359^{+0.274}_{-0.044}$	$0.269^{+0.044}_{-0.021}$
zedge2	$E_c$ (keV)	$0.712^{+0.011}_{-0.013}$	$1.054^{+0.041}_{-0.045}$	$0.713^{+0.012}_{-0.006}$	$1.071^{+0.053}_{-0.062}$	$0.751^{+0.020}_{-0.023}$	$0.714^{+0.011}_{-0.012}$
	$\tau$	$0.147^{+0.030}_{-0.022}$	$0.033^{+0.013}_{-0.014}$	$0.072^{+0.013}_{-0.010}$	$0.029^{+0.019}_{-0.011}$	$0.045^{+0.013}_{-0.007}$	$0.063^{+0.012}_{-0.012}$
zedge3	$E_c$ (keV)	$1.122^{+0.126}_{-0.094}$	$1.231^{+0.038}_{-0.039}$	$1.160^{+0.019}_{-0.018}$	$1.231^{+0.159}_{-0.087}$	$1.217^{+0.033}_{-0.031}$	$1.127^{+0.021}_{-0.019}$
	$\tau$	$0.022^{+0.023}_{-0.022}$	$0.047^{+0.015}_{-0.014}$	$0.086^{+0.013}_{-0.007}$	$0.023^{+0.020}_{-0.018}$	$0.057^{+0.014}_{-0.014}$	$0.072^{+0.011}_{-0.011}$
Simpl	$\Gamma$	$2.474^{+0.024}_{-0.023}$	$2.513^{+0.014}_{-0.013}$	$2.418^{+0.014}_{-0.008}$	$2.495^{+0.018}_{-0.017}$	$2.448^{+0.019}_{-0.009}$	$2.428^{+0.015}_{-0.014}$
	FracScat	$0.193^{+0.008}_{-0.007}$	$0.192^{+0.004}_{-0.005}$	$0.153^{+0.004}_{-0.004}$	$0.194^{+0.006}_{-0.006}$	$0.152^{+0.005}_{-0.005}$	$0.151^{+0.004}_{-0.004}$
nthComp	$\Gamma$	$2.295^{+0.052}_{-0.047}$	$2.292^{+0.010}_{-0.019}$	$2.676^{+0.059}_{-0.050}$	$2.353^{+0.016}_{-0.022}$	$2.795^{+0.063}_{-0.055}$	$2.862^{+0.051}_{-0.044}$
	kT(keV)	$0.184^{+0.020}_{-0.020}$	$0.195^{+0.009}_{-0.008}$	$0.220^{+0.027}_{-0.020}$	$0.192^{+0.011}_{-0.010}$	$0.240^{+0.032}_{-0.023}$	$0.254^{+0.031}_{-0.022}$
	Norm	$0.014^{+0.0008}_{-0.0009}$	$0.012^{+0.0003}_{-0.0003}$	$0.011^{+0.0004}_{-0.0003}$	$0.013^{+0.0004}_{-0.0003}$	$0.015^{+0.0005}_{-0.0004}$	$0.011^{+0.0004}_{-0.0003}$
red $\chi^2$ /d.o.f.		1.03/149	1.58/161	1.62/160	1.17/158	1.03/159	1.30/164
Model	Parameter	0670130501	0006810301	0206400101	0670130701	0670130401	
zedge1	$E_c$ (keV)	$0.346^{+0.006}_{-0.007}$	$0.338^{+0.006}_{-0.007}$	$0.513^{+0.006}_{-0.006}$	$0.587^{+0.045}_{-0.037}$	$0.341^{+0.008}_{-0.018}$	
	$\tau$	$0.406^{+0.039}_{-0.044}$	$0.595^{+0.226}_{-0.226}$	$0.093^{+0.008}_{-0.009}$	$0.035^{+0.019}_{-0.020}$	$0.303^{+0.041}_{-0.041}$	
zedge2	$E_c$ (keV)	$0.718^{+0.012}_{-0.009}$	$0.489^{+0.012}_{-0.012}$	$0.706^{+0.005}_{-0.007}$	$0.716^{+0.013}_{-0.011}$	$0.710^{+0.009}_{-0.005}$	
	$\tau$	$0.069^{+0.011}_{-0.011}$	$0.188^{+0.024}_{-0.017}$	$0.116^{+0.011}_{-0.012}$	$0.126^{+0.017}_{-0.024}$	$0.075^{+0.012}_{-0.012}$	
zedge3	$E_c$ (keV)	$1.197^{+0.023}_{-0.020}$	$0.710^{+0.015}_{-0.017}$	$1.111^{+0.018}_{-0.019}$	$1.143^{+0.023}_{-0.027}$	$1.164^{+0.030}_{-0.032}$	
	$\tau$	$0.068^{+0.012}_{-0.012}$	$0.102^{+0.017}_{-0.016}$	$0.054^{+0.009}_{-0.009}$	$0.061^{+0.014}_{-0.014}$	$0.046^{+0.011}_{-0.011}$	
Simpl	$\Gamma$	$2.437^{+0.011}_{-0.014}$	$2.376^{+0.009}_{-0.012}$	$2.472^{+0.009}_{-0.004}$	$2.436^{+0.016}_{-0.016}$	$2.416^{+0.012}_{-0.015}$	
	FracScat	$0.144^{+0.004}_{-0.004}$	$0.085^{+0.015}_{-0.015}$	$0.183^{+0.003}_{-0.003}$	$0.183^{+0.004}_{-0.005}$	$0.159^{+0.005}_{-0.004}$	
nthComp	$\Gamma$	$2.892^{+0.029}_{-0.029}$	$3.127^{+0.024}_{-0.021}$	$2.381^{+0.019}_{-0.022}$	$2.175^{+0.022}_{-0.027}$	$2.748^{+0.049}_{-0.051}$	
	kT(keV)	$0.250^{+0.032}_{-0.023}$	$0.240^{+0.006}_{-0.004}$	$0.188^{+0.009}_{-0.008}$	$0.191^{+0.009}_{-0.008}$	$0.233^{+0.032}_{-0.022}$	
	Norm	$0.012^{+0.0004}_{-0.0002}$	$0.009^{+0.00003}_{-0.0001}$	$0.010^{+0.0001}_{-0.0003}$	$0.009^{+0.0002}_{-0.0003}$	$0.011^{+0.0003}_{-0.0003}$	
red $\chi^2$ /d.o.f.		1.35/163	1.16/148	1.62/165	1.51/163	1.49/164	

described the data well at a few percentage level and most of the discrepancies are at low energies. The high energy photon index is not too sensitive to the actual model used as we show later when we fit only the high energy part (3-10 keV) of the spectra and obtain qualitatively similar results. Nevertheless, we caution against over-interpretation of the best fit values obtained in these fits, especially for the components affecting the low energy part of the spectra.

#### 4 THE EFFECT OF COMPLEX ABSORPTION AND REFLECTION COMPONENT

The spectra of Mrk 335, may be affected by complex absorption and there may be a relativistically blurred reflection component which may dominate at low and high energies. Given the quality of the data many of these complex models may be degenerate, however in the present context it is useful to quantify the effect of these models on the high energy spectral index. The motivation here is not to obtain a physically self consistent model but rather to understand their effect of the high energy spectral index and hence in the primary result of this work.

To take into account the possibility of complex absorption, we include in the phenomenological model, partial ionised absorber represented by the XSPEC routine “zxipcf” (Miller et al. 2007). The absorption is characterised by three parameters namely the column density, the covering fraction and the ionisation parameter of the absorber. For the addition of three parameters the changes in  $\chi^2$  for the four high flux observations with IDs 0101040101,0306870101,

0600540601 and 0600540501 were 12.7, 22.0, 3.1, 9.0 and 12.0 respectively. More importantly, the best fit high energy spectral indexes obtained were  $2.05 \pm 0.05$ ,  $1.78 \pm 0.06$ ,  $1.75 \pm 0.05$  and  $1.81 \pm 0.02$ . When compared with the high energy spectral indexes obtained from the phenomenological model, one can see that the errors are larger and any change in the index is less than 0.1. In contrast, for the deep low flux state, ID 0510010701, the  $\Delta\chi^2 = 45$  and the spectral index obtained was  $1.55 \pm 0.15$  which is significantly different from the phenomenological model.

Next we consider the possible effect of a complex relativistically blurred reflection component in the spectra. Since, the ionised reflection component produces a complex soft excess which needs to be modelled with absorption, we limit our analysis to energies  $> 2$  keV. This is adequate since our interest here is to study the effect of the component on the high energy index. Since for the phenomenological model, the spectra shows the presence of a narrow and broad Iron lines, we consider a power-law and two reflection components represented by the table model “reflionx” (Ross & Fabian 2005). For one of the the reflection component we convolve it using the relativistic blurring model “kdblur” where we fix the inner and outer radii, but allow for the emissivity index to be free. The best fit power-law index for the four high flux state observations with IDs 0101040101,0306870101, 0600540601 and 0600540501 were  $2.09 \pm 0.05$ ,  $2.16 \pm 0.02$ ,  $1.77 \pm 0.03$  and  $1.64 \pm 0.05$ . We note that for the observation with ID. 0306870101 the change in spectral index as compared to the phenomenological model is  $\sim 0.28$  while for the others it is  $< 0.15$ . For the deep low flux state, ID 0510010701, the spectral index obtained was

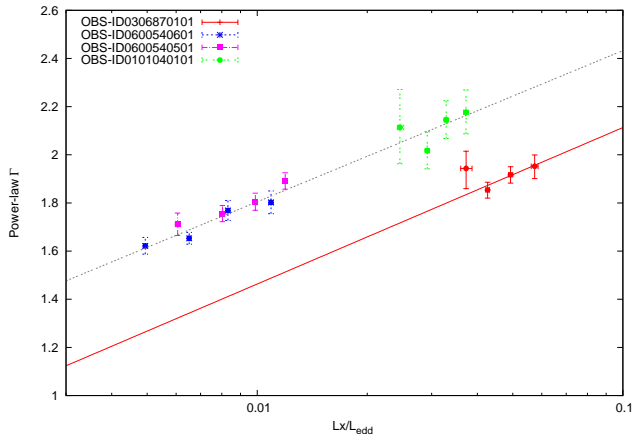


**Figure 4.** The high energy photon index,  $\Gamma$  versus the X-ray Eddington ratio for Mrk 335. The X-ray Eddington ratio is  $L_X/L_{Edd}$  where  $L_X$  is the unabsorbed luminosity in the 0.3-10 keV range. The solid line is a fit to three of the data sets and has a slope  $m = 0.64 \pm 0.04$  and intercept  $c = 3.08 \pm 0.08$  with a reduced  $\chi^2 = 0.57$ . The bottom dotted straight line is a fit only to the data set (ID0306870101) and has a slope  $m = 0.65 \pm 0.04$  and intercept  $c = 2.76 \pm 0.07$  with a reduced  $\chi^2 = 0.76$ .

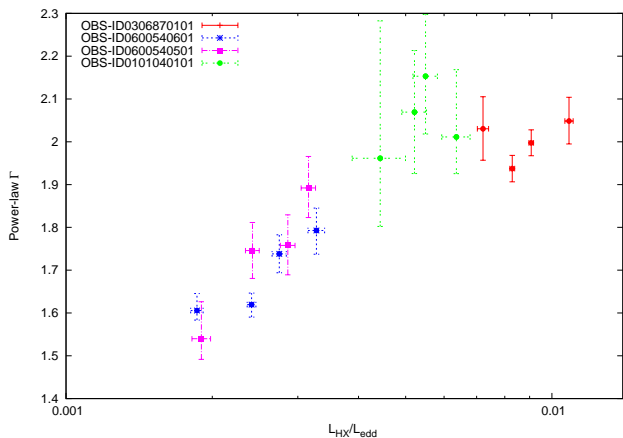


**Figure 5.** Same as Figure 4 except that only the energy range 3-10 keV is taken into account. The spectra are fitted with a power-law and Iron line. The luminosity  $L_{HX}$  corresponds to the energy range 3-10 keV. Note the similarity with Figure 4 which implies that the qualitative results are not sensitive to the spectral model adopted.

$3.00 \pm 0.07$  which is radically different than the value obtained earlier.

Thus, the effect of complex absorption or reflection is dramatic for the deep low state. This is expected based on the analysis of Grupe et al. (2008). For the other higher flux states, complex absorption may change the index by  $< 0.1$  from those of the phenomenological model. The effect of Complex reflection on the index is also modest  $< 0.15$  but we note that it may be large  $\sim 0.28$  for the observation with

ID. 0306870101, which incidentally is also the highest flux state in the sample.

## 5 FLUX-RESOLVED SPECTROSCOPY

The light curves for each of the observations of Mrk 335 and Ark 564 are shown in Figure 2 and Figure 3 which reveals that for nearly all observations there is significant flux variation in timescales of  $\sim 10^4$  s. To investigate the variation of the photon index, each observation was split into 3 or 4 flux levels (marked by horizontal dotted lines in Figures 2 and 3) and the corresponding spectrum was generated. We do not consider the 2007 observation of Mrk 335 (ID0510010701) for the flux resolved spectroscopy since as shown in the previous section the spectra is clearly complex and the phenomenological model used here is not adequate.

Each of the flux level spectra was fitted with the same phenomenological model used for the average spectra. However, due to the lower statistics of the flux resolved spectra, there were several parameters which were either not constrained or were consistent within error bars to be not varying during the observations. Thus, several spectral parameters were fixed to their best fit values obtained from the fitting of the average spectra. These were, the energies of the different edges and emission lines, the temperature and normalisation of the soft photon Comptonization (i.e.  $kT_{bb}$  and normalisation of the “nthcomp” component) and the normalisation and emissivity index of the Iron line (i.e.  $\beta$  and normalisation of the “diskline” component).

For each flux resolved spectra, the unabsorbed flux in the 0.3-10 keV band was computed using the XSPEC model “cflux”. The fluxes were converted into luminosities,  $L$  by using the luminosity distances of 103 Mpc for Mrk 335 and 98.5 Mpc for Ark 564, which are the average values quoted in the NED website. For Mrk 335, the black hole mass was taken to be  $1.4 \times 10^7 M_\odot$  (Peterson et al. 2004; Grier et al. 2012) while for Ark 564 we adopt a value of  $2.61 \times 10^6 M_\odot$  (Botte et al. 2004) to obtain their respective Eddington luminosities  $L_{Edd}$ . The best fit parameters for the flux resolved spectra are listed in Table 4.

In this work we consider the X-ray Eddington ratio i.e.  $L_X/L_{Edd}$  instead of the Bolometric one and discuss the implication of this in the last section. In Figure 4, the high energy photon index is plotted against the X-ray Eddington ratio for the different flux resolved spectra. Three of the observations cover an order of magnitude range in X-ray Eddington ratio from 0.004 to 0.04 and show a tight correlation between the photon index and X-ray Eddington ratio. A straight line fit to these three observation sets gives a slope  $m = 0.64 \pm 0.04$ , intercept  $c = 3.08 \pm 0.08$  and reduced  $\chi^2 = 0.57$ . The observation with the highest X-ray Eddington ratio  $> 0.04$ , does not follow the linear relation. Instead fitting the flux resolved spectra for that observation only, one gets a straight line with slope  $m = 0.65 \pm 0.04$ , intercept  $c = 2.76 \pm 0.07$  and reduced  $\chi^2 = 0.76$ . In other words, the data follows a parallel track. Note that the lowest luminosity observation ( $L_X/L_{Edd} \sim 0.002$ ) was not included in the straight line fit. Nevertheless, the fit to the high flux data, passes through the lowest flux one.

To verify that the results do not depend sensitively on the phenomenological spectral model used, we repeat the flux resolved spectroscopy analysis using only the energy band 3-10 keV. We fit this energy band with a power-law and

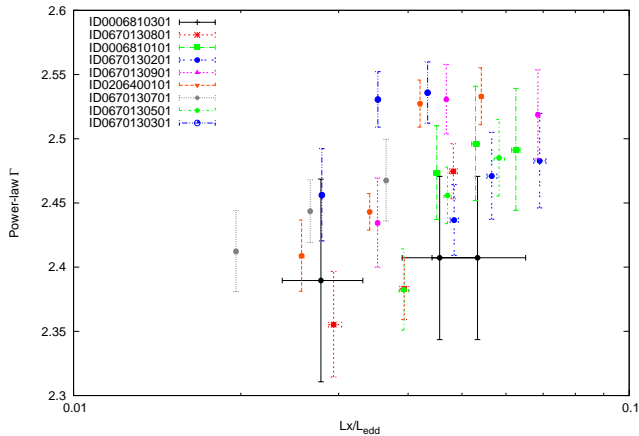


**Figure 6.** The high energy photon index,  $\Gamma$  versus the X-ray Eddington ratio for Ark 564. The X-ray Eddington ratio is  $L_X/L_{Edd}$  where  $L_X$  is the unabsorbed luminosity in the 0.3-10 keV range.

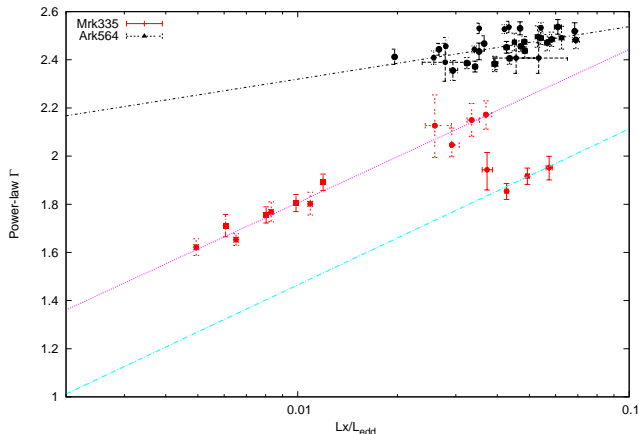


**Figure 7.** Summary figure for the high energy photon index,  $\Gamma$  versus the X-ray Eddington ratio for both Mrk 335 and Ark 564. The X-ray Eddington ratio is  $L_X/L_{Edd}$  where  $L_X$  is the unabsorbed luminosity in the 0.3-10 keV range. For Mrk 335 two parallel tracks are observed with a possible switching at  $L_X/L_{Edd} \sim 0.04$ , while for Ark 564 the correlation is flatter and with significantly more scatter.

a broad Iron line. Figure 5 shows the results of this analysis where the photon index is plotted against  $L_{HX}/L_{Edd}$ , where  $L_{HX}$  is computed using the unabsorbed flux in the 3-10 keV band.

Figure 6 shows the results of the flux resolved analysis (for the complete 0.3-10 keV band) for Ark 564. Here, despite the larger number of observations, the flux variation is modest with the X-ray Eddington ratio ranging from 0.02-0.07. Although there is more scatter than the case of Mrk 335, there is a correlation between the spectral index and X-ray Eddington ratio. A straight line fit gives a slope  $m = 0.22 \pm 0.08$ , intercept  $c = 2.75 \pm 0.1$  and a large reduced  $\chi^2 = 2.75$ . From the Figure, it seems that for the flux resolved spectra of each individual observation the correlation may be better and perhaps the different observations are parallelly shifted with respect to each other. However, the statistics is not good enough to make any concrete statements.

## 6 DISCUSSION

Figure 7 summarises the results of the work by showing the variation of the high energy photon index versus the X-ray Eddington ratio for both Mrk 335 and Ark 564. For Mrk 335, there are two parallel tracks with the possibility that the sources shifts to the lower track for  $L_X/L_{Edd} > 0.04$ . For Ark 564 the points are clustered at a larger  $\Gamma$  and while there is a positive correlation, the slope is flatter and points show much more scatter than the points for Mrk 335.

It should be noted that the luminosity used in this work is in the energy range 0.3-10 keV and is not the bolometric one and hence these results cannot be compared directly with those where the bolometric luminosity or X-ray luminosity in some other energy range has been used. The conversion to Bolometric luminosity often involves several uncertain factors and hence is avoided in this work. Since for Mrk 335, we find the the index correlates well with the X-ray luminosity for nearly an order of magnitude change in luminosity, this may indicate that over this range the bolometric correction is nearly constant. On the other hand, it may well be that for this source the X-ray index correlates better with the X-ray luminosity and not with the bolometric one. The uncertainties and model dependency of estimating the bolometric luminosity (including the general non-availability of simultaneous multi-wavelength data) does not allow for concrete statements. For Mrk 335, there is only one observation for which the X-ray Eddington ratio is larger than 0.04 and the source follows a lower parallel track. It is necessary to confirm this behaviour with future observations when the source is equally luminous. It might be that there is a real transition at the X-ray Eddington ratio  $\sim 0.04$  or that the source can actually follow any of the two tracks at the same luminosity.

In the Comptonization context, the high energy power-law index is inversely proportional to the Compton Amplification factor  $A$ , which is the ratio of the luminosity of Comptonizing cloud,  $L_c$  to the input soft photon luminosity  $L_{inp}$  i.e.  $A = L_c/L_{inp}$ . The input luminosity  $L_{inp}$  depends on the luminosity of the soft photon source and the fraction of photons which enter the Comptonizing region. The latter depends on the accretion geometry of the system. Thus, the correlation between the photon index and the observed luminosity could occur if  $A$  decreases with luminosity or in other words  $L_c$  varies less rapidly with the observed luminosity than  $L_{inp}$ . The shift to the lower parallel track can be explained if there is a decrease in  $L_{inp}$  at the X-ray Eddington ratio of  $\sim 0.04$ , perhaps caused by a change in the fraction of photons entering the Comptonizing region. This would mean that the accretion geometry for the two parallel tracks are different.

The high energy photon index could also be affected by the presence of a strong reflection component, especially if the reflection is from partially ionised matter and/or is relativistically blurred such that it has a significant contribution to the spectra below 10 keV. The reflection component would tend to flatten the high energy spectrum and hence the correlation may be caused by the reflection component decreasing as the source becomes more luminous. Indeed, the anomalous low luminosity observation of Mrk 335 of July 2007, can be modelled as being dominated by a blurred reflection component (Grupe et al. 2008). It may also be that



the primary correlation between the index and luminosity is due to variation of the Compton Amplification factor, while the shift to a different parallel track is due to appearance of a strong reflection component. The appearance of a stronger reflection component would also mean that there was a change in the accretion disk geometry. Thus, a qualitative change in the accretion disk geometry seems to be required to explain the parallel tracks seen for Mrk 335. Changes in the accretion disk geometry at the same X-ray luminosity seems to indicate that the accretion flow is not determined only by the local accretion rate but rather it may also depend on the previous history of the accretion rate variation. Our brief analysis of including a blurred reflection component suggests that this indeed may be the case. It is particularly interesting to note that for the highest flux observation (ID 101040101) a reflection component may increase the index by 0.28 while a more modest variation is expected for the others (Section 4). If indeed this highest flux observation has a stronger reflection component and its spectral index is more close to  $\sim 2$  then it would seem that the index has a positive correlation with flux but saturates to  $\sim 2$  at high Eddington ratios. Interestingly a similar behavior is observed in Fig. 5, where the results for a simple power law plus Iron line fit to the 3-10 keV energy range are shown. However, this can be confirmed only with broad band data covering energies  $> 10$  keV where the reflection component will be better constrained.

The results for Ark 564 are significantly different than that for Mrk 335, with a flatter correlation and more scatter. This suggests that the behaviour of AGNs is not homogeneous and perhaps cannot be understood by studying a large sample of them. Long term sensitive and broad band monitoring of individual AGNs may be expected to provide better insights.

## ACKNOWLEDGMENTS

RS acknowledges IUCAA visitor program and AP acknowledges seed money grant from Tezpur University and visiting associateship IUCAA, Pune. This research made use of data obtained from the High Energy Astrophysics Science Archive Research Center (HEASARC), provided by NASA's Goddard Space Flight Center. The authors would like to thank the anonymous referee for useful suggestions which has enhanced the quality of the paper.

## REFERENCES

- Arnaud K., ASP Conf.Ser.101:Astronomical Data Analysis Software and Systems, 101, 1996, 17
- Barth A. J., Greene J. E., Ho L. C., 2005, ApJ, 619, L151
- Boller T., Brandt W. N. & Fink H., 1996, A&A, 305, 53
- Boroson T. A., 2002, ApJ, 565, 78
- Brandt W. N., Mathur S. & Elvis M., 1997, MNRAS, 285, 15
- Brightman M. et al. 2013, MNRAS, 433, 2485
- Botte V., Ciroi S., Rafanelli P. & Mille Dr. F., 2004, AJ, 127, 3168
- Cao X.-W. 2009, MNRAS, 394, 207
- Chiang J. et al., 2000, ApJ, 528, 292
- Collin S., Kawaguchi T., Peterson B. M., Vestergaard M., 2006, A&A, 456, 75
- Constantin A., Green P., Aldcroft T. et al., 2009, ApJ, 705, 1336
- Done C., Madejski G. M. & Życki P. T. 2000, ApJ, 536, 213
- Dewangan G. C., Boller th., Singh K.P. & Leighly K.M., 2002, A&A, 390, 65
- Dewangan G. C., Griffiths R. E., Dasgupta S. & Rao, A. R., 2007, ApJ, 671, 1284
- Fabian A.C., Rees M. J., Stella L. & White N.E., 1989, MNRAS, 238, 729
- Gu, M. & Cao, X., 2009, MNRAS, 399, 349
- Gallo L. C., Boller T., Tanaka Y., Fabian A. C., Brandt W. N., Welsh W. F., Anabuki N., Haba Y., 2004, MNRAS, 347, 269
- Gallo L.C. et al., 2013, MNRAS, 428, 1191
- Grier et al., 2012, ApJ, 744, 4
- Grupe D., 2004, AJ, 127, 1799
- Grupe D., Komossa S., Gallo L.C., Fabian A., Larsson J., Pradhan A.K., Xu D. & Miniutti G., 2008a, ApJ, 681, 982
- Grupe D., Komossa S., Gallo L.C., Longinotti A. L., Fabian A., Pradhan A.K., Gruberbauer M. & Xu D. APJS, 2012, 199, 17
- Gondoin P., Orr A., Lumb D. & Santos-Lleo M., 2002, A&A, 388, 74
- Haardt F. & Maraschi L. 1991, ApJ, 380, 51
- Haardt F. & Maraschi L. 1993, ApJ, 413, 507
- Huchra J. P., Vogeley M. S. & Geller M. J. 1999, ApJS, 121, 287
- Jansen F. et al. 2001, A&A, 365, 1
- Jin C., Ward M. & Done C., 2012, MNRAS, 425, 907
- Kalberla P.M.W., Burton W. B., Hartmann Dap, Arnal E. M., Bajaja E., Morras R.W. & Pppel W. G., 2005, A&A, 440, 775
- Komossa S., 2008, RMxAC, 32, 86
- Komossa S., Xu D., 2007, ApJ, 667, L33
- Larsson J., Miniutti G., Fabian A. C., Miller J. M., Reynolds, C.S. & Ponti G., 2008, MNRAS, 384, 1316
- Laor A., Fiore F., Elvis M., Wilkes B. J. & McDowell J. C., 1997, ApJ, 477, 93
- Legg E., Miller L., Turner T. J., Giustini M., Reeves J. N. & Kraemer S. B., 2012, ApJ, 760, 73
- Leighly K. M., 1999, ApJS, 125, 317
- Liu J. Y., Liu B. F., Qiao E. L. & Mineshige S., 2012, ApJ, 754, 81
- Longinotti A. L., Sim S. A., Nandra K. & Cappi M., 2007, MNRAS, 374, 237
- Lu Y. & Yu Q., 1999, ApJL, 526, 5
- Mushotzky R. M., Done C., Pounds K. A., 1993, ARA&A 31, 717
- Miller L., Turner T. J., Reeves J. N., George I. M., Kraemer S. B., Wingert B., 2007, A&A, 463, 131
- Nandra K. & Pounds K. A., 1994, MNRAS, 268, 405
- Nandra K., Le T., George I. M., Edelson R. A., Mushotzky R. F., Peterson B. M. & Turner T. J., 2000, ApJ, 544, 734
- Nandra K., & Papadakis I. E., 2001, ApJ, 554, 710
- Osterbrock D. E., Pogge R. W., 1985, ApJ, 297, 166
- O'Neill P. M., Nandra K., Cappi M., Longinotti A. L. & Sim S.A., 2007, MNRAS 381, 94
- Page K. L., Reeves J. N., O'Brien P. T. & Turner M. J. L.,

- 2005, MNRAS, 364, 195
- Papadakis I. E., Brinkmann W., Page M. J., McHardy I. & Uttley, P. 2007, A&A, 461, 931
- Perola G. C. et al., 1986, ApJ, 306, 508
- Peterson B.M., et al., 2004, ApJ, 613, 682
- Porquet D., Reeves J. N., OBrien P. & Brinkmann W. 2004, A&A, 422, 85
- Risaliti G., Young M. & Elvis M., 2009, ApJ, 700, 6
- Romano P., Mathur S., Turner T. J. et al. 2004, ApJ, 602, 635
- Ross R. R., Fabian A. C., 2005, MNRAS, 358, 211
- Saez C., Chartas G., Brandt W. N., Lehmer B. D., Bauer F. E., Dai X. & Garmire G. P. 2008, AJ, 135, 1505
- Singh K. P., Rao A. R. & Vahia M. N., 1991, A&A, 248, 37
- Struder, L., Briel U., Dennerl K., et al., 2001, A&A, 365, 18
- Steiner J. F., Narayan R., McClintock J. E., & Ebisawa K., 2008, PASP, 121, 1279
- Shemmer O., Romano P., Bertram R., et al. 2001, ApJ, 561, 162
- Shemmer O., Brandt W. N., Netzer H., Maiolino R., Kaspi S., 2006, ApJL, 646, 29
- Sobolewska M. A. & Papadakis I. E. 2009, MNRAS, 399, 1597
- Tananbaum H et al., 1978, ApJ, 223, 74
- Turner T. J., Romano P., George I. M., et al. 2001, ApJ, 561, 131
- Vignali C., Brandt W. N., Boller T., Fabian A. C., Vaughan S., 2004, MNRAS, 347, 854
- Vaughan S. & Edelson R., 2001, ApJ, 548, 694
- Véron-Cetty M.-P., Véron P., Gonçalves A. C., 2001, A&A, 372, 730
- Warner C., Hamann F., Dietrich M., 2004, ApJ, 608, 136
- Wang J. M., Watarai K. Y. & Mineshige S., 2004, ApJ, 607, 107
- Williams R. J., Pogge R. W., Mathur S., 2002, AJ, 124, 3042
- Williams R. J., Mathur S., Pogge R. W., 2004, ApJ, 610, 737
- Xu Ya-Di, 2011, ApJ, 729, 10
- Xu D. W., Komossa S., Wei J. Y., Qian Y., Zheng X. Z., 2003, ApJ, 590, 73
- Yaqoob T. & Warwick R. S., 1991, MNRAS, 248, 773
- Younes G., Porquet D., Sabra B. & Reeves J. N., 2011, A&A, 530, 149
- Zdziarski A. A., Poutanen J. & Johnson W. N., 2000, ApJ, 542, 703
- Zdziarski A.A & Grandi P., 2001, ApJ, 551, 186
- Zhou Xin-Lin & Zhao Yong-Heng, 2010, ApJ, 720, 206

**Table 4.** Spectral parameters for each flux state (for Mrk 335 & Ark 564) derived from different *XMM-Newton* observations in the (0.3-10.0)keV range. The full version is available to download online

Obs ID	flux state	zedge1	zedge2	zedge3	Simpl		nthComp	red $\chi^2$ /d.o.f.
		$\tau$	$\tau$	$\tau$	$\Gamma$	FracScat	$\Gamma$	
0101040101 (Mrk 335)	1	$0.002 \times 10^{-4+908.7}$ $-0.002$	$0.073^{+0.101}$ $-0.065$	-	$2.114^{+0.157}$ $-0.151$	$0.140^{+0.039}$ $-0.030$	$2.979^{+0.125}$ $-0.190$	0.92/ 82
	2	$0.132^{+0.055}$ $-0.055$	$0.024^{+0.055}$ $-0.024$	-	$2.017^{+0.078}$ $-0.076$	$0.120^{+0.016}$ $-0.013$	$2.780^{+0.096}$ $-0.084$	1.01/120
	3	$0.098^{+0.055}$ $-0.055$	$0.074^{+0.053}$ $-0.053$	-	$2.145^{+0.080}$ $-0.077$	$0.140^{+0.020}$ $-0.017$	$2.921^{+0.127}$ $-0.106$	0.89/120
	4	$0.077^{+0.063}$ $-0.063$	$0.070^{+0.061}$ $-0.061$	-	$2.177^{+0.093}$ $-0.090$	$0.160^{+0.028}$ $-0.022$	$2.896^{+0.162}$ $-0.127$	1.05/112
0006810101 (Akn 564)	1	$0.107^{+0.041}$ $-0.041$	$0.121^{+0.046}$ $-0.046$	$-0.006^{+0.037}$ $-0.036$	$2.473^{+0.037}$ $-0.036$	$0.189^{+0.013}$ $-0.012$	$2.401^{+0.085}$ $-0.076$	0.93/137
	2	$0.093^{+0.048}$ $-0.048$	$0.127^{+0.054}$ $-0.054$	$0.041^{+0.044}$ $-0.044$	$2.496^{+0.045}$ $-0.044$	$0.197^{+0.017}$ $-0.015$	$2.289^{+0.093}$ $-0.083$	0.99/130
	3	$0.124^{+0.051}$ $-0.052$	$0.199^{+0.059}$ $-0.059$	$0.045^{+0.047}$ $-0.047$	$2.491^{+0.048}$ $-0.047$	$0.204^{+0.018}$ $-0.016$	$2.177^{+0.092}$ $-0.082$	1.05/126